Decoding the spectra of SDSS early-type galaxies: New indicators of age and recent star formation

Ben Rogers[1], Ignacio Ferreras[1,2]⋆, Ofer Lahav[2], Mariangela Bernardi[3], Sugata Kaviraj[4] and Sukyoung K. Yi[5]

[1] *Department of Physics, King's College London, Strand, London WC2R 6LS*
[2] *Department of Physics and Astronomy, University College London, Gower St. London WC1E 6BT*
[3] *Department of Physics and Astronomy, University of Pennsylvania, USA*
[4] *Astronomy group, The Denys Wilkinson Building, Keble Road, Oxford, OX1 3RH*
[5] *Centre for Space Astrophysics, Yonsei University, Seoul, South Korea*

arXiv:0709.0300v1 [astro-ph] 3 Sep 2007

ABSTRACT

We apply Principal Component Analysis (PCA) to a sample of early-type galaxies from the Sloan Digital Sky Survey (SDSS) in order to infer differences in their star formation histories from their unresolved stellar populations. We select a $z < 0.1$ volume-limited sample comprising ~ 7000 early-type galaxies from SDSS/Data Release 4. Out of the first few principal components (PC), we study four which give information about stellar populations and velocity dispersion. We construct two parameters (η and ζ) as linear combinations of PC1 and PC2. The four components can be presented as "optimal filters" to explore in detail the properties of the underlying stellar populations. By comparing various photo-spectroscopic observables – including NUV photometry from GALEX – we find ζ to be most sensitive to recent episodes of star formation, and η to be strongly dependent on the average age of the stellar populations. Both η and ζ also depend on metallicity. We apply these optimal filters to composite spectra assembled by Bernardi et al. The distribution of the η component of the composites appear to be indistinguishable between high and low density regions, whereas the distribution of ζ parameters have a significant skew towards lower values for galaxies in low density regions. This result suggests that galaxies in lower density environments are *less* likely to present weak episodes of recent star formation. In contrast, a significant number of galaxies from our high density subsample – which includes clusters (both outer regions and centres) and groups – underwent small but detectable recent star formation at high metallicity, in agreement with recent estimates targeting elliptical galaxies in Hickson Compact Groups and in the field (Ferreras et al.).

Key words: galaxies: elliptical and lenticular, cD – galaxies: evolution – galaxies: formation – galaxies: stellar content.

1 INTRODUCTION

Observational studies of galaxy formation follow a two-pronged approach. On the one hand dynamical studies relate to the past mass assembly history of galaxies. We believe this history is strongly driven by the "bottom-up" hierarchical merging scenario as predicted by the ΛCDM paradigm by which massive halos form from the progressive mergers of smaller systems. Massive cosmological simulations computed within the ΛCDM framework give large scale properties in agreement with available surveys (Springel et al. 2005).

On the other hand, the star formation history tracks the trans-formation of gas into stars, a process controlled both by the merging structure described above as well as by the highly non-linear physics of star formation. Even full-fledged cosmological models of structure formation have to rely on simple prescriptions of star formation as the dynamical range required for a consistent treatment is far beyond the current capabilities of numerical simulations (see e.g. De Lucia et al. 2006). The complexity of star formation and its possible feedback mechanisms represent our current bottleneck in numerical studies of galaxy formation and justify alternative approaches aimed at extracting information about the star formation history from photo-spectroscopic properties of the unresolved stellar populations.

The pioneering work of Tinsley (see e.g. Tinsley 1980) was based on a comparison of well-defined models of galaxy formation

including stellar evolution with photometric data in order to assess the ages and metallicities of galaxies. This work was continued by more detailed population synthesis models (e.g. Bruzual & Charlot 2003). The age-metallicity degeneracy (Worthey 1994) by which age and metallicity effects generate similar photo-spectroscopic trends represent the main hurdle constraining the star formation history of galaxies. This problem is more severe when dealing with the old stellar populations found in early-type galaxies. Subsequent work targeting age-sensitive absorption lines (Worthey & Ottaviani 1997; Vazdekis & Arimoto 1999; Trager et al. 2000) is arguably the best approach to quantifying differences between stellar populations, although caveats exist (see e.g. Prochaska et al. 2007).

Other approaches aim at using as much information as possible (namely the whole spectral energy distribution), but comparisons are hindered by the sheer volume of parameter space to be explored. Ingenious approaches (Heavens, Jimenez & Lahav 2000; Panter, Heavens & Jimenez 2003; Ocvirk et al. 2006) have been proven useful to decipher the star formation histories of galaxies but there are uncertainties as to the accuracy of the parameters extracted by the models. The effect of systematics – such as flux calibration errors – can translate into large uncertainties on the estimates of the stellar ages.

Multivariate techniques such as Principal Component Analysis or Independent Component Analysis (Hyvärinen, Karhunen & Oja 2001) follow a different approach. Instead of a direct comparison between data and models, the observations are considered to be the sole source of information. These data are classified or rearranged in a way that maximises the amount of information (in the sense of variance) carried by the spectra. The models are used "a posteriori" to put the physics back in. The advantage of this approach is that trends seen on the rearranged spectra (i.e. the principal components, independent components, hidden variables, etc) are robust and model-independent.

PCA has been previously applied to various sets of astrophysical spectra; from stars (Deeming 1964) to active galactic nuclei (Francis, Hewett, Foltz & Chaffee 1992). Most notably, PCA has allowed the classification of galaxy spectra from surveys such as 2dF (Madgwick et al. 2003) and SDSS (Yip et al. 2004). Our approach is different. We use PCA not as a classification tool for a wide range of spectra, but as a method to extract minute differences in the stellar populations of an otherwise highly homogeneous sample. Our work is a continuation of the pioneering studies of Faber (1973) and more recent work on SDSS galaxies by Eisenstein et al. (2003).

These multivariate techniques have been mainly applied to the classification or compression of spectra (e.g. Yip et al. 2004). Recently, these techniques have been pursued on galaxy data with another purpose: to extract differences in the underlying stellar populations in order to determine the star formation histories. For that purpose, elliptical galaxies represent one of the best systems. These galaxies pose a well-known problem: dominated by old stellar populations – for which the time evolution is very slow – they present a strong age-metallicity degeneracy (Ferreras, Charlot & Silk 1999).

At the same time, these galaxies represent one of the best places to constrain our knowledge of galaxy assembly. Massive ellipticals are dominated by old stars, suggesting an old, brief and intense period of star formation (the so-called monolithic collapse). However, our understanding of structure formation requires these galaxies to be assembled later on via massive mergers. Even though semi-analytic models improve and give reasonable answers to this problem (Kaviraj et al. 2005; De Lucia et al. 2006; Kaviraj et al. 2007), the models do not have enough resolution to target important

issues related to star formation. For instance, the alpha-enhanced values measured in massive ellipticals are still a matter of controversy in the light of hierarchical models (Thomas 1999). The star formation prescriptions used by semi-analytic models (see e.g. Croton et al. 2006) are clearly insufficient to account for the effects that cause these overabundances. Furthermore, the effect of environment on the stellar populations is also an important issue: hierarchical models predict significant differences in the star formation histories of galaxies with respect to local density. In essence, galaxies in denser regions form earlier (Sheth & Tormen 2004). However, detailed spectroscopic observations do not show large differences in the stellar populations of field and cluster ellipticals (Bernardi et al. 1998; 2006).

Recent studies applying various multivariate techniques (Kabán, Nolan & Raychaudhury 2005; Ferreras et al. 2006; Nolan, Raychaudhury & Kabán 2007) to the spectra of early-type galaxies have started to give very valuable insight into the underlying stellar populations of these systems. This information is gathered in a total independent way to model-oriented techniques. Hence, this methodology of tackling the star formation history of unresolved stellar populations is becoming a valuable complement to studies based on equivalent widths.

2   THE SAMPLE

Our sample is extracted from the catalogue of Bernardi et al. (2006) which comprises ∼42,000 elliptical and lenticular galaxies selected from the Sloan Digital Sky Survey (York et al. 2000). From this starting catalogue, we select a volume-limited sample to redshift $z < 0.1$. We examine a plot of redshift versus absolute magnitude (in the r band) of the original sample to determine the cut to be imposed on the absolute magnitude for a $z < 0.1$ sample. We find this cut to be at $M_r < -20.7$. Furthermore, we impose a limit of S/N⩾ 15 to avoid noisy spectra. The cut in S/N results in a small fraction of galaxies at the faint end to be rejected but within Poisson error bars we tested that no significant bias is introduced.

The preliminary sample comprises 9192 galaxies. These galaxies are compared with the luminosity function of early-type galaxies measured in SDSS (Nakamura et al. 2003) to find that a further cut at $M_r \leqslant -21$ should be imposed to obtain a volume-limited sample. Our final sample thereby comprises 7148 galaxies out to $z < 0.1$ and brighter than $M_r \leqslant -21$. The characteristic luminosity from the Schechter function fit to SDSS early-type galaxies is $M_r(\star) = -21.6$. Hence, our galaxies correspond to $L_r \geqslant 0.6L_{r,\star}$. The average redshift of the sample is $\langle z \rangle = 0.075$.

The SEDs were extracted from Data Release 5 (Adelman-McCarthy et al. 2007). The spectra were dereddened – using the Fitzpatrick (1999) $R_v = 3.1$ Galactic extinction curve, taking the reddening values from the maps of Schlegel, Finkbeiner & Davis (1998) – and deredshifted using a linear interpolation algorithm and the redshift estimates supplied by SDSS. Finally, the SEDs were normalised to the same average flux across the 6000-6500Å wavelength range.

3   PRINCIPAL COMPONENT ANALYSIS AS A TOOL TO REARRANGE GALACTIC SPECTRA

Principal Component Analysis (PCA) is a multivariate technique aimed at reducing the dimensionality of a data set in order to decrease the complexity of the analysis. Each member of the sample

(a galaxy SED in our case) is defined by an "information vector", an N-tuple of numbers given by the flux measured at a set of wavelengths: $\{\Phi(\lambda_i)\}, i = \{1, 2, \cdots N\}$. PCA consists of decorrelating sets of vectors by performing rotations in the n-dimensional parameter space spanned by the wavelength bins. The final result is a diagonal covariance matrix, with the eigenvalues representing the amount of information (in the sense of variance) stored in each eigenvector, which is called a principal component. Rearranging the principal components in decreasing order allows us to determine the main ones that contribute to determine the information vectors of the input spectra.

Details of the PCA technique for our specific problem can be found elsewhere (Ferreras et al. 2006). Notice that in our methodology we do not subtract the mean from each of the input vectors, i.e. we do not eliminate the average spectrum. This implies the matrix we are diagonalising is not the covariance matrix. As stated in Ferreras et al. (2006), subtracting the mean removes information from PCA, specifically about the shape of the continuum, which would be preferable to keep within the analysis. Since the sample used here is restricted to early-type galaxies, for which only small differences are apparent between spectra, the mean and first eigenvector, e_1 should be similar. PCA done with such mean subtraction indeed confirms this idea. A more orthodox "mean-subtracted" PCA is well justified in cases such as the classification of 2dF spectra (Madgwick et al. 2003), where the subtraction of the mean alleviates the strong uncertainties in their flux calibration. Nevertheless we performed PCA both with and without mean-subtraction on our sample to find no significant difference in the outcome. The net effect is, roughly, a shift in the rank of the principal components, so that e_2 becomes e_1 in the mean-subtracted version, etc.

We apply PCA to different "flavours" of the observed data. In order to assess the robustness of the extraction of the components we compare the projections of the galaxy spectra on to the principal components obtained in several different ways. We present the spectra to PCA for several wavelength ranges: 3850–4150Å(just encompassing the 4000Å break); 3850–4400Å(including information from the G-band); 3850–5000Å (our fiducial wavelength range); and finally continuum-subtracted spectra (using a 200Å boxcar median filter to determine the continuum) over the 3850–5000Å range. The results from these different sets of spectra allow us to assess whether flux calibration errors can introduce a systematic effect. We decided not to extend our analysis to wavelengths redder than rest-frame $\lambda = 5000$Å as many of the SDSS spectra suffer from a poorly subtracted night sky line (OI $\lambda = 5577$Å). PCA is very sensitive to outliers, which contribute excessively to the variance. Furthermore, the region around the night sky line cannot be simply masked out as the position of this line gets deredshifted along with the galaxy spectra to different wavelengths depending on the redshift of each galaxy. We tried various methods, including a replacement of the region around the emission line with a normalized average of all the spectra, but the results were not satisfactory. In order to make our results as robust as possible we decided not to tresspass the 5000Å limit, which keeps the 5577Å OI night sky line safely away from the spectra of all of our $z < 0.1$ galaxies.

Flux calibration errors can have an effect on the projected components. Blind techniques such as PCA rely heavily on data which should have systematic effects kept under control. Data gathered from various sources can yield results directly related to differences in the systematics of these sources. By choosing a homogeneous sample (SDSS DR5) we minimise such effects. Furthermore, the SDSS errors of flux calibration are stated to be limited

Table 1. Weight of the first Principal Components

Label	Spectral Range	λ_1(%)	λ_2(%)	λ_3(%)
1	3850–4150Å	99.183	0.072	0.019
2	3850–4400Å	99.425	0.055	0.015
3	3850–5000Å	99.693	0.067	0.006
4	CS^{a}3850–5000Å	69.305	0.880	0.336

^{a} CS = Continuum Subtracted.

to ∼3% (see www.sdss.org/dr4/algorithms/fluxcal). We find flux calibrations of this order not to give any strong differences in the projected components presented here.

Table 1 shows the "weight" of the first few principal components. PCA applied to the full spectra gives a dominant first principal component (a result of the high homogeneity of the stellar populations in early-type galaxies). The strength of this first component increases as the wavelength range is increased. In contrast, the continuum subtracted spectra give a more spread out distribution of weights among the first principal components. However, the first component still dominates the variance.

The first Principal Components obtained both with the full SEDs and with the continuum subtracted ones are shown in figure 1. The first component shows the characteristic features of old stellar populations, a prominent 4000Å break and no Balmer absorption. The calcium H and K lines are also visible along with the G band, clear indicators of cool stars. The second component can be physically attributable to a young stellar population, with prominent Balmer absorption and a blue continuum. Its low variance (∼ 0.07%) is consistent with the lack of young stars in early-type galaxies. Our first and second principal components are analogous to the $a1$ and $a2$ components of Nolan et al. (2007), who used factor analysis to decompose the spectral information from a sample of early-type galaxies from SDSS/DR4. Our third principal component is notably noisier than the first two, but notice the next components do not appear as noisy. We will show below that the third component correlates strongly with the velocity dispersion, a property that appears throughout the SED, hence its noisy appearance. Of the higher order components it is worth mentioning the fifth component, which clearly presents the Balmer series. This component is remarkably similar to the one obtained by applying PCA to a smaller sample of early-type systems in the field and in Hickson Compact Groups (Ferreras et al. 2006; Ferreras et al. 2006b). However, the sample studied here is several orders of magnitude larger and the Balmer lines appear at a higher S/N ratio. The very low variance associated to this component (around 0.002%) implies Balmer-strong spectra – i.e. the so-called E+A or k+A galaxies – are not common in a large, low-redshift, volume-limited sample of early-type systems such as the one presented here. The sample selection done by Bernardi et al. (2006) do not bias in any way against the selection of this type of galaxies, hence the low variance associated to this component should reflect the weight of these post-starburst galaxies in the census of $z < 0.1$ early-type systems, in contrast with the population of such systems at moderate and high-redshift (Tran et al. 2003). We should emphasize that the long-range structure seen in high order components such as e_4 or e_6 is not physical, but an artifact generated by the enforced orthogonality of the principal components.

The panels on the right hand side of figure 1 show the principal components for the continuum-subtracted spectra. The features are

harder to interpret, but the calcium H+K lines, the G band and some of the Balmer absorption lines are evident.

Figure 2 gives the projections of the galaxies on the first two principal components for different options of the spectral range or for the continuum subtracted spectra (as labeled in table 1). The figure shows that these different "flavours" give very similar projections of the galaxy spectra on to the principal components, i.e. the decomposition is fairly robust, and the results do not change significantly even when the information from the continuum is subtracted. Henceforth, we will use the data with the maximum amount of information, namely the full SED over the wavelength range 3850–5000Å .

3.1 Projected Components

The principal components can be considered a set of basis vectors that optimally filter the information hidden in the spectra. We can rearrange the information hidden in the N components $\{\Phi(\lambda_i)\}$, $i = \{1, 2, \cdots N\}$ by projecting the SEDs on to the principal components. This is equivalent to a rotation in the N-dimensional parameter space spanned by the wavelength sampling.

$$\mathrm{PC1}_i = \vec{\Phi}_i \cdot \vec{e}_1 = \sum_{j=1}^{N} \Phi_i(\lambda_j) e_1(\lambda_j), \qquad (1)$$

and analogously for PC2, PC3, etc. According to the sharply decreasing eigenvalues, one would expect most of the information (in the sense of variance) to stay in the first few principal components.

Figure 3 shows the projection of the spectra of all galaxies in our sample on components 1, 2, 3 and 5. Given the number of galaxies to be plotted, we present the figure as a greyscale corresponding to the density of galaxies. For those regions with lower densities in PC parameter space, we replace the greyscale by dots representing the projections of individual galaxies. The projections of the first two components, PC1 and PC2, show a correlation, present both in the full SED (bottom left) as well as in the continuum-subtracted one (bottom right). This result is consistent with the analysis of the smaller sample comprising field and Hickson Compact Group galaxies (Ferreras et al. 2006). We tested against a bias caused by S/N by comparing separate projections of the galaxies with high and low S/N to find the same trend. The projections of the higher order components do not show any significant correlation with PC1 or PC2, althogh we find the outliers in the PC1 vs PC5 diagram to be galaxies with very prominent Balmer lines (i.e. post-starburst galaxies). Notice the remarkably small fraction of such systems found with high projections of PC5 in this large volume-limited sample.

The bottom-left panel of figure 3 also shows a simple linear fit to the data. In the same spirit as the decomposition done by Madgwick et al. (2003) on the PC1-PC2 plane spanned by their sample of 2dF galaxies, we rotate the PC1-PC2 plane into two independent components η (the length of the projection along the straight line that describes the fit) and ζ (the distance to the line). As shown in Ferreras et al. (2006), such a definition allows us to enhance the mapping between principal components and actual physical parameters.

Figure 4 compares the projection of the principal components with a set of physical observables such as redshift, absolute magnitude, velocity dispersion or colour (as measured inside the fibre used for the extraction of the spectra). There are two sets of panels corresponding to the analysis of the full spectra (left) and the continuum-subtracted version (right). Each figure shows in grey the

projections of the galaxy spectra on to the principal components, as well as the binned average and variance. The figure illustrates the clear correlation between PC1,PC2 and colour, to be expected in the full spectra as the principal components correspond to a red and blue spectrum, respectively. However, it is quite remarkable to find such a strong correlation for the continuum-subtracted case, where this colour information has been removed when presenting the spectra to PCA. It is also worth mentioning the strong correlation found between PC3 and velocity dispersion. A similar correlation appears in PC1 and PC2, however we believe such is an indirect effect caused by the well-known relation between velocity dispersion and colour (see e.g. Bernardi 2003; 2005). No strong correlation is apparent with PC5. Since PC5 is associated to Balmer absorption, one could again interpret this result as the lack of important "activity" regarding post-starburst spectra in the $z < 0.1$ universe. The correlation between projections PC2 and PC5 and a young stellar component is also illustrated in figure 5 where a combination of both projections are compared with the equivalent width of Hδ_A (as defined in Worthey & Ottaviani 1997); and the 4000Å break (as defined in Balogh et al. 1999).

Quantitatively, we present least-squares fits to these data in table 2. We show for each fit the slope and intercept as well as Pearson's linear correlation coefficient r (see e.g. Press et al. 1992). Furthermore, we give an estimate labelled "Pred." as the predictability of each physical observable using the fit to a given principal component. This number gives the RMS of the distribution $(X_{\mathrm{fit}} - X_{\mathrm{obs}})/X_{\mathrm{obs}}$, for every physical observable X. Notice the strongest correlation appears between PC3 and velocity dispersion, with a predictability of $\sim 4\%$ and between PC1,PC2 with colour, retrieving the observed colours within a 10% error.

4 COMPARISON WITH A MAXIMUM LIKELIHOOD METHOD

The advantage of PCA lies in its ability to extract the components that hold most of the information (in the sense of variance) in a model independent way. The principal components presented above do not relate to any prescription regarding population synthesis or galaxy formation. Unfortunately this also implies that in order to put the "physics" back in, one has to compare the components or the projections with models. Our main goal is to relate the projections for our sample of galaxies with estimates of age or metallicity of the underlying stellar populations.

We compare our galaxies with a set of synthetic spectra using the stellar population models of Bruzual & Charlot (2003). We assume an exponentially decaying star formation rate (i.e. a τ model). Each star formation history (SFH) is described by three parameters, namely the metallicity Z – kept fixed at all times; the time at which star formation starts (which we can relate to a formation redshift z_F); and the timescale τ that controls the star formation rate. For each SFH we convolve the simple stellar populations – using a Chabrier (2003) IMF – into a composite spectrum which is smoothed to the same velocity dispersion of the galaxy and sampled in the same way as the SDSS spectra. A χ^2 is computed and the parameters corresponding to a maximum likelihood is searched in a $24 \times 24 \times 24$ grid over a wide range of the parameters:

$$0.1 \leqslant Z/Z_\odot \leqslant 2$$
$$0 \leqslant \log(z_F) \leqslant 1$$
$$0.1 \leqslant \tau/\mathrm{Gyr} \leqslant 6.$$

The best fit is subsequently improved by a Metropolis method

Table 2. Linear fits of the Principal Component projections to some physical observables

Y	X	Slope	Cut	r^1	Pred.^{2}
PC1$\times10^3$	$\log\sigma$	-5.071	45.365	-0.178	0.206
PC2$\times10^3$	$\log\sigma$	-4.341	9.827	-0.426	0.080
PC3$\times10^3$	$\log\sigma$	$+2.033$	-4.624	$+0.685$	0.039
PC5$\times10^3$	$\log\sigma$	-0.339	0.770	-0.189	0.197
PC1$\times10^3$	M_r	$+0.214$	38.462	$+0.045$	0.522
PC2$\times10^3$	M_r	$+0.303$	6.512	$+0.181$	0.131
PC3$\times10^3$	M_r	-0.201	-4.347	-0.411	0.052
PC5$\times10^3$	M_r	$+0.055$	1.199	$+0.188$	0.126
PC1$\times10^3$	$\log R_e$	-2.365	35.004	-0.030	0.692
PC2$\times10^3$	$\log R_e$	-0.673	0.286	-0.024	0.898
PC3$\times10^3$	$\log R_e$	$+0.298$	-0.147	$+0.036$	0.578
PC5$\times10^3$	$\log R_e$	$+0.027$	-0.014	$+0.005$	3.913
PC1$\times10^3$	$g-r$	-27.049	54.287	-0.570	0.095
PC2$\times10^3$	$g-r$	-9.763	7.335	-0.578	0.099
PC3$\times10^3$	$g-r$	$+0.880$	-0.665	$+0.179$	0.384
PC5$\times10^3$	$g-r$	$+0.367$	-0.278	$+0.123$	0.567

[1] Pearson's linear correlation coefficient (see e.g. Press et al. 1992, pg. 636).
[2] This is the RMS of the *predictability* of the fit to reproduce the physical observable X from the measurement of the component Y (see text for details).

where extra models are randomly sampled and an accept/reject criterion based on the likelihood is used to properly sample the probabilily distribution of the parameters (see e.g. Saha 2003). Here we use the best fit values for the metallicity and the average age (which is a function of z_F and τ). The best fits for these galaxies have a mean $\langle\chi^2_r\rangle = 0.9$ with RMS= 0.3, a typical sign of the degeneracies present in analyses of unresolved stellar populations. Synthetic models fit "too well" and it is very hard to disentangle these degeneracies.

Figure 6 shows contours of the projections of the model spectra on to the principal components. They are shown in the 2D parameter space spanned by either average age and metallicity (*left*, assuming a fixed velocity dispersion of $\sigma = 200$ km s^{-1}), or average age and velocity dispersion (*right*, assuming solar metallicity). The dashed line shows the contours with the highest value of the projection in each case. The age-metallicity degeneracy (see e.g. Worthey 1994) is apparent in the figure: one cannot choose a set of parameters whose contours cross in a way to univocally determine the value of age and metallicity. For instance, η and ζ have very similar dependence with age and metallicity. PC5 – which features the characteristic Balmer absorption lines – appears to be more sensitive to age than metallicity, a well-known fact exploited as the method to estimate ages from Balmer indices (see e.g. Worthey & Ottaviani 1997; Vazdekis & Arimoto 1999). Notice η and ζ are insensitive to velocity dispersion. The strong dependence of PC3 on the velocity dispersion of the models shown in the right-hand panels of figure 6 is consistent with the observed correlation between PC3 and σ shown in figure 4. The observed correlation between PC1,PC2 and velocity dispersion (table 2) is caused by the intrinsic correlation between σ and colour (see e.g. Bernardi et al. 2003).

Figure 7 compares subsets of galaxies with a given age and metallicity – estimated by the maximum likelihood method described above – in the parameter space spanned by our principal components. The figure show as grey dots the projections of the total sample and as black dots those galaxies corresponding to different age and metallicity distributions. The top panels correspond

to old ages ($\langle t\rangle \geqslant 12$Gyr) and the bottom panels are best fit by younger populations ($\langle t\rangle \leqslant 9$Gyr). Left and right panels are separated with respect to metallicity, as labelled.

Notice that the dependence of η and ζ with respect to metallicity is very different for old and young populations. As we change the metallicity of young stars, the ζ parameter increases without a strong change in η, whereas a range in metallicity in old stellar populations has an effect both in η and ζ. This will be an important trend to bear in mind when UV fluxes are taken into account (in the next section).

An alternative set of models to compare with the spectra consist of a young (simple) stellar population added to an overall old component. This two-burst method is motivated by the idea of "frostings" of young stars over an otherwise old population (Trager et al. 2000) and has been succesfully used to explore recent star formation in elliptical galaxies (Ferreras & Silk 2000; Kaviraj et al. 2007; Schawinski et al. 2006). Figure 8 shows a comparison with these models. The old component is a τ-model with a formation redshift $z_F = 5$ and star formation timescale $\tau = 1$ Gyr. Three parameters are explored to find the best fit: the age (t_Y) and mass fraction (f_Y) of the young component; and the metallicity of the galaxy –which is assumed to be the same for both old and young components to reduce the number of free parameters. Using the same technique as described above, we show in the figure the results for the η and ζ projections. The grey dots correspond to the whole sample, whereas we show as black dots those galaxies whose spectral fitting requires a significant "frosting". We chose those with $f_Y/t_Y > 0.01$, which implies e.g. a 1% contribution in 1 Gyr stars or a 0.1% contribution in 100 Myr stars. These galaxies populate the region corresponding to a higher value of η and ζ. We emphasize here that these are just simple models to guide our analysis based on the principal components. The real galaxies – which we will explore in more detail in the next section – have a distribution of stellar populations much more complicated than any of the simple models described here (or elsewhere). Hence the advantage of multivariate, model independent, analysis.

5   COMPARISON WITH NEAR ULTRAVIOLET PHOTOMETRY

Photons detected from early-type galaxies in the ultraviolet spectral window come from two main sources: evolved Horizontal Branch stars and their progeny or recent episodes of star formation (O'Connell 1999). The former are responsible for the UV upturn around 1200Å and it was not clear until recently whether near ultraviolet (NUV) light could be only attributed to evolved stars in early-type galaxies. The recent survey of SDSS early-type galaxies targeted by GALEX (Yi et al. 2005) confirmed that a small albeit measurable recent star formation (RSF) is present in a significant number of early-type galaxies. The observed flux in the near ultraviolet passband of GALEX centered at 2350Å is most sensitive to hot dwarfs and even though there can be some contribution from evolved HB stars, the NUV$-r$ colours observed in many of the targeted ellipticals cannot be explained purely by an old population. Schawinski et al. (2006) estimate that galaxies with colours NUV$-r < 5.4$ must have a fraction of young stars. This fraction can be as small as a few percent (Kaviraj et al. 2007) and it is not clear what causes this episode of star formation.

Our sample of 7148 galaxies includes 921 objects that overlap with the GALEX Medium Imaging Survey (Morrissey et al. 2005). For details on the photometry we refer to Schawinski et al. (2006) and Kaviraj et al. (2007). In order to enhance the contrast between NUV bright and NUV faint galaxies, we select those with NUV$-r \leqslant 4.9$ as blue galaxies and NUV$-r \geqslant 5.9$ as red galaxies. The subsamples comprise 151 blue and 241 red galaxies. The mean redshift of both subsamples is $\langle z \rangle = 0.076$, compatible with the average redshift of our sample (0.075). Figure 9 shows the histogram of the projections of these two subsamples on our principal components. The distribution of η, PC3 and PC5 are indistinguishable, whereas the histogram corresponding to ζ features a significant skew towards higher values for the blue subsample. In the light of the comparison with synthetic models it is remarkable to find such a result given that the estimated amount of recent star formation stays below a few percent (Kaviraj et al. 2007). Furthermore, instead of NUV, we are using the less sensitive optical spectral window to detect such effect. This illustrates the power of PCA to extract small differences from the spectral energy distribution. This result allows us to further relate the ζ parameter to recent star formation. Notice that figure 6 show that *both* η and ζ depend on age (and metallicity), whereas the comparison with GALEX data suggest ζ to be the only parameter sensitive to recent star formation.

The bottom panels of figure 9 show the histograms of PC1 and PC2 for the continuum-subtracted spectra. The separation is much harder to determine, however a slight difference can be seen in the histograms of PC2 (in analogy with ζ for the full SED case). Even though this result is very weak, it is quite remarkable given that the information regarding colours is completely eliminated when subtracting the continuum.

The lines in the top panels correspond to simple models overlaying a young (0.5 Gyr) population over an old component (12 Gyr), for three different metallicities as labelled. The lines correspond to a change in f_Y, the stellar mass fraction in young stars. Notice the difference in the predicted evolution of η and ζ as f_Y is increased. The lines illustrate that a small "frosting" (as in Trager et al. 2000) in young, metal-rich stars can increase the value of ζ without a large change in η. Hence ζ is the parameter most sensitive to recent (and small) episodes of star formation as long as the

metallicity is high. More intense star formation stages (or at lower metallicity) would reflect in changes both for η and ζ.

6   COMPARISON WITH THE COMPOSITE SPECTRA OF BERNARDI ET AL.

In order to compare our results with the more established method focussing on the equivalent widths of some absorption lines with strong age or metallicity trends (e.g. Worthey & Ottaviani 1997; Kuntschner & Davies 1998; Vazdekis & Arimoto 1999; Trager et al. 2000; Thomas & Maraston 2003; Bernardi et al. 2003) we apply the composite spectra of Bernardi et al. (2006). These models were generated from the original sample from which our catalogue is extracted. Galaxies were arranged in bins of redshift, absolute magnitude, velocity dispersion, etc... and combined to generate composite SEDs with a S/N high enough for an analysis of equivalent widths. We refer the reader to Bernardi et al. (2006) for a detailed study of these composite spectra.

Figure 10 shows a comparison between the projections of the composite SEDs on our principal components and the age and metallicity estimates obtained from an analysis of spectral lines including Hγ_A. Only those models with our redshift ($z \leqslant 0.1$) and absolute magnitude ($M_r < -21$) limits were considered. The triangles and error bars give the mean and standard deviation of data binned in age or metallicity. The figure shows the dependence of the projections on both age and metallicity. High values of η and ζ correspond to younger stellar ages. However, the interplay between age and metallicity is complicated and one can find – consistently with figure 7 – that a high value of η can be a signature of younger ages or lower metallicities. Only when η changes without a strong change in ζ can we disentangle the effects and associate the SED with recent star formation (as in the NUV bright/faint separation shown above).

7   DISCUSSION AND CONCLUSIONS

With the comparison between the projections of the galaxy spectra on to the principal components and their relationship with physical observables such as those obtained from synthetic spectra (§4) or NUV photometry (§5) we can put some physics back into the analysis. PCA reduces most of the information – in the sense of variance – to a biparametric set defined by η and ζ. This result is reminiscent of the work of Faber (1973). We have found that a variation of the ζ component can disentangle the effect of small amounts of young star formation as long as the young burst corresponds to high metallicities. This effect is apparent in a comparison of the distributions of the η and ζ projections for NUV bright and faint galaxies as in figure 9.

No significant effect is found regarding the fact that our spectra are extracted from a fibre, which will map different physical sizes at different redshifts. From the lowest redshift found in our sample ($z = 0.03$) to the $z = 0.1$ limit imposed, the $3''$ diameter of the fibre covers a physical size from 1.8 to 5.5 kpc. However, the steep surface brightness profile of early-type systems and the not-too-deep exposure of the fibres implies that most of the light from the observed spectra comes from the inner regions of these galaxies regardless of redshift. We compared the projections of the principal components η and ζ as well as the higher order ones, to find no significant trend with redshift. For instance, the difference in the distribution of η and ζ found between NUV-bright and faint galaxies

– shown in figure 9 – is preserved when subsamples with redshift only below (or above) the median redshift are chosen. Hence we conclude our analysis is insensitive to aperture effects.

We can extend this analysis to the composite spectra of Bernardi et al. (2006). Among various properties, these models are binned according to average density. Hence, we can separate these composite models into high- and low-density galaxies depending on whether the distance to the nearest cluster *and* the distance to the 10th nearest neighbour are both smaller or greater than 10 Mpc, respectively. The distributions of the projections of the high/low density composite spectra on the principal components are shown in figure 11. In parallel to the comparison with NUV$-r$ colours (figure 9) we find no significant difference in the distributions of η, PC3 and PC5, whereas ζ presents a skew towards higher values for galaxies in our higher density regions *analogous to NUV$-r$ blue galaxies*. Our "high-density bin" includes galaxies across a wide range of environments: from groups to clusters: both central regions and outskirts. In this paper we show that early-type galaxies in *low density regions* do NOT present those signs of recent star formation, compared to their counterparts in higher density regions (cf. Denicoló et al. 2006; Clemens et al. 2006; Schawinski et al. 2006; de la Rosa et al. 2007). An ongoing project will explore the environmental issue in more detail (Ferreras et al., in preparation). Nevertheless, from the data presented in this paper we can safely conclude that environmental effects are very small in early-type galaxies: PCA finds a departure from a homogeneous stellar population across different environments of less than 1%.

These results confirm the minor effect that the environment seems to play on the star formation histories of early-type galaxies, in agreement with previous work (see e.g. Bernardi et al. 1998; Smith et al. 2006). Nevertheless, the difference between the high and the low-density distributions is significant: A Kolmogorov-Smirnov test comparing the 268 high-density composites and the 314 low-density composites give a KS statistic of D=0.145 and 0.237 for η and ζ, respectively, implying a statistical significance of over 99% that both samples do NOT come from the same distribution. In order to strengthen this point, we show in figure 12 a Monte Carlo test. We perform 10000 comparisons between subsamples of 100 spectra each. The solid line shows the distribution of the D-statistic from the Kolmogorov-Smirnov test when applied between subsamples in high and low-density regions, whereas the grey, dashed line histograms correspond to comparisons between subsamples obtained from the same density bin, or from the whole set of composites. Both η and ζ are clearly split when comparing subsamples in different density regions, but the latter shows a very strong separation.

The interpretation of the mild correlation would suggest galaxies in higher density regions (most likely groups and the outskirts of clusters) to have weak episodes of recent star formation at high metallicity. These high metallicities are to be expected in the heavily polluted interstellar medium of an early-type galaxy. This result is consistent with a recent analysis of a smaller sample comprising early-types both in Hickson Compact Groups and in the field (Ferreras et al. 2006). In this sample, galaxies in groups present a stronger second principal component compared to elliptical galaxies in the field, i.e. frostings of recent star formation. It is interesting to contrast this result with Nolan et al. (2007) who find E+A 'post-starburst' galaxies (not-necessarily with an early-type morphology) mainly in group/field environments, with a significant decrease at higher densities. In combination with the analysis presented in this paper, the data hint at a peak in the (frostings) activity of early-type galaxies at group densities. The weakness of these star formation episodes is also consistent with the small amount of cold gas that could survive in this type of galaxies (Faber & Gallagher 1976). There is recent evidence from a CO emission survey targeting SAURON early-type galaxies which suggests that these episodes of star formation should be fuelled by the infall of small amounts of gas from the outside (Combes, Young & Bureau 2007). The fraction in young stars is estimated to be a few percent, which is so small as to challenge model-dependent methods.

REFERENCES

Adelman-McCarthy, J. K., et al., 2007, ApJS, submitted
Balogh, M. L., Morris, S. L., Yee, H. K. C., Carlberg, R. G., Ellingson, E. 1999, ApJ, 527, 54
Bernardi, M., et al. 1998, ApJ, 508, L143
Bernardi, M., et al. 2003, AJ, 125, 1882
Bernardi, M., et al. 2005, AJ, 129, 61B
Bernardi, M., et al. 2006, AJ, 131, 1288
Bruzual, G., Charlot, S., 2003, MNRAS, 344, 1000
Clemens, M.S., et al. 2006, MNRAS, 370, 702
Combes, F., Young, L. M. & Bureau, M., 2007, astro-ph/0703557
Croton, D. J., et al. 2006, MNRAS, 365, 11
Deeming T. J., 1964, MNRAS, 127, 493
de la Rosa, I. G., de Carvalho, R. R., Vazdekis, A. & Barbuy, B., 2007, AJ, 133, 330
De Lucia, G., Springel, V., While, S. D. M., Croton, D., Kauffmann, G., 2006, MNRAS, 366, 499
Denicoló, G., Terlevich, R., Terlevich, E., Forbes, D. A. & Terlevich, A., 2006, MNRAS, 358, 813
Eisenstein, D. J., et al. 2003, ApJ, 585, 694
Faber, S. M., 1973, ApJ, 179, 731
Faber, S. M. & Gallagher, J. S., 1976, ApJ, 204, 365
Ferreras, I., Charlot, S. & Silk, J., 1999, ApJ, 521, 81
Ferreras, I. & Silk, J., 2000, ApJ, 541, L37
Ferreras, I., Pasquali, A., de Carvalho, R. R., de la Rosa, I. G., Lahav, O., 2006, MNRAS, 370, 828
Ferreras, I., Rogers, B. & Lahav, O., 2006b, astro-ph/0611456
Fitzpatrick, E. L., 1999 PASP, 111, 63
Folkes, S.R., Lahav, O., Maddox, S. J., 1996, MNRAS, 283, 651
Francis, P. J., Hewett, P. C., Foltz, C. B., Chaffee, F. H., 1992, ApJ, 398, 476
Heavens, A. F., Jimenez, R. & Lahav, O., 2000, MNRAS, 317, 965

Hyvärinen, A., Karhunen, J. & Oja, E., 2001, *Independent Component Analysis*, Wiley, New York.

Kabán, A., Nolan, L. A. & Raychaudhury, S., 2005, SIAM 2005 International Conference on Data Mining, astro-ph/0505059

Kaviraj, S., Devriendt, J. E. G., Ferreras, I. & Yi, S. K., 2005, MNRAS, 360, 60

Kaviraj, S., et al., 2007, ApJ, accepted (astro-ph/0601029)

Kuntschner, H. & Davies, R. L., 1998, MNRAS, 295, L29

Lacey, C. & Cole, S., 1994, MNRAS, 271, 676

Madgwick, D., et al, 2003, MNRAS, 343, 871

Morrissey, P., 2005, ApJ, 619, L7

Nakamura, O., et al. 2003, AJ, 125, 1682

Nolan, L. A., Raychaudhury, S. & Kabán, A., 2007, MNRAS, 375, 381

O'Connell, R. W., 1999, ARA& A, 37, 603

Ocvirk, P., Pichon, C., Lançon, A. & Thibaut, E., 2006, MNRAS, 365, 74

Padmanabhan, N., 2004, NewA, 9, 329

Panter, B., Heavens, A. F. & Jimenez, R., 2003, MNRAS, 343, 1145

Press, W. H., Teukolsky, S. A., Vetterling, W. T., & Flannery, B. P. 1992, Numerical Recipes in C (Cambridge: Cambridge Univ. Press).

Prochaska, L. C. et al., 2007, astro-ph/0702589

Ronen, S., Aragón-Salamanca, A., Lahav, O., 1999, MNRAS, 303, 284

Rood H. J., Struble, M. F., 1994, PASP, 106, 413

Ronen, S., Aragón-Salamanca, A., Lahav, O., 1999, MNRAS, 303, 284

Saha, P., 2003, Principles of Data Analysis (Great Malvern: Cappella Archive)

Schlegel, D. J., Finkbeiner, D. P., Davis, M., 1998, ApJ, 500, 525

Schawinski, K., et al., 2006, ApJ, in press, astro-ph/0601036

Sheth, R. K. & Tormen, G., 2004, MNRAS, 350, 1385

Slonim, N., Somerville, R., Tishby, N., Lahav, O., 2001, MNRAS, 323, 270

Smith, R. J., Hudson, M. J., Lucey, J. R., Nelan, J. E. & Wegner, G. A., 2006, MNRAS, 369, 1419

Springel, V., et al. 2005, Nature, 435, 629

Thomas, D. 1999, MNRAS, 306, 655

Thomas, D. & Maraston, C., 2003, A& A, 401, 429

Tinsley, B. M. 1980, Fund. Cosm. Phys., 5, 2877

Trager, S. C., Faber, S. M., Worthey, G. & Gonzlez, J. J, 2000, AJ, 120, 165

Tran, K.-V. H., Franx, M., Illingworth, G., Kelson D. D. & van Dokkum, P., 2003, ApJ, 599, 865

Vazdekis, A. & Arimoto, N., 1999, 525, 144

Worthey, G., 1994, ApJS, 95, 107

Worthey, G., Ottaviani, D.L., 1997, ApJ, 111, 377

York, D. G., et al., 2000, AJ, 120, 1579

Yi, S. K., et al. 2005, ApJ, 619, L111
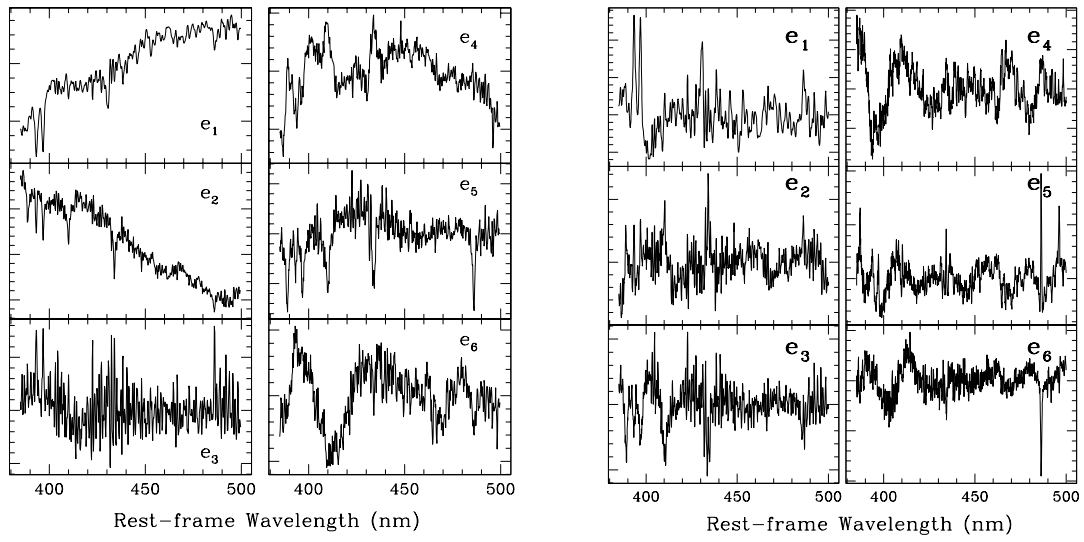
Yip, C. W., et al., 2004, AJ, 128, 2603

Figure 1. The first six principal components using the full SED (*left*) and the continuum subtracted SED (*right*), over the wavelength range 3850–5000Å . These components correspond to "flavours" 3 (left) and 4 (right) in table 1. The projection ("dot product") of these eigenvectors ($e_1, e_2, \cdots$) with each galaxy is denoted throughout the paper as PC1, PC2, etc.
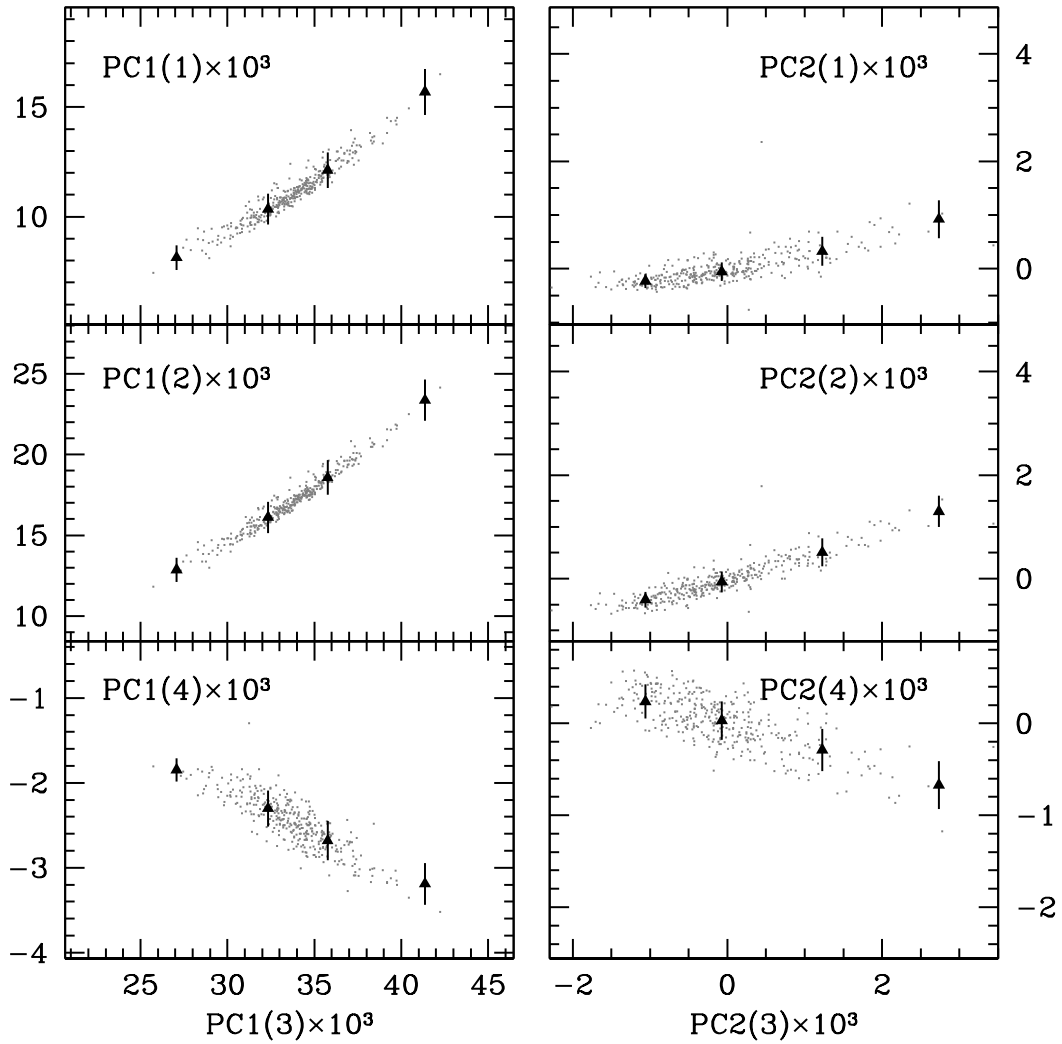
Figure 2. Comparison between the projection of the sample galaxies on the first two principal components for four different "flavours" of the spectra as explained in the text. The indices in brackets correspond to those in table 1. The black triangles and error bars are the average and median of the samples binned in PC1(3) and PC2(3).
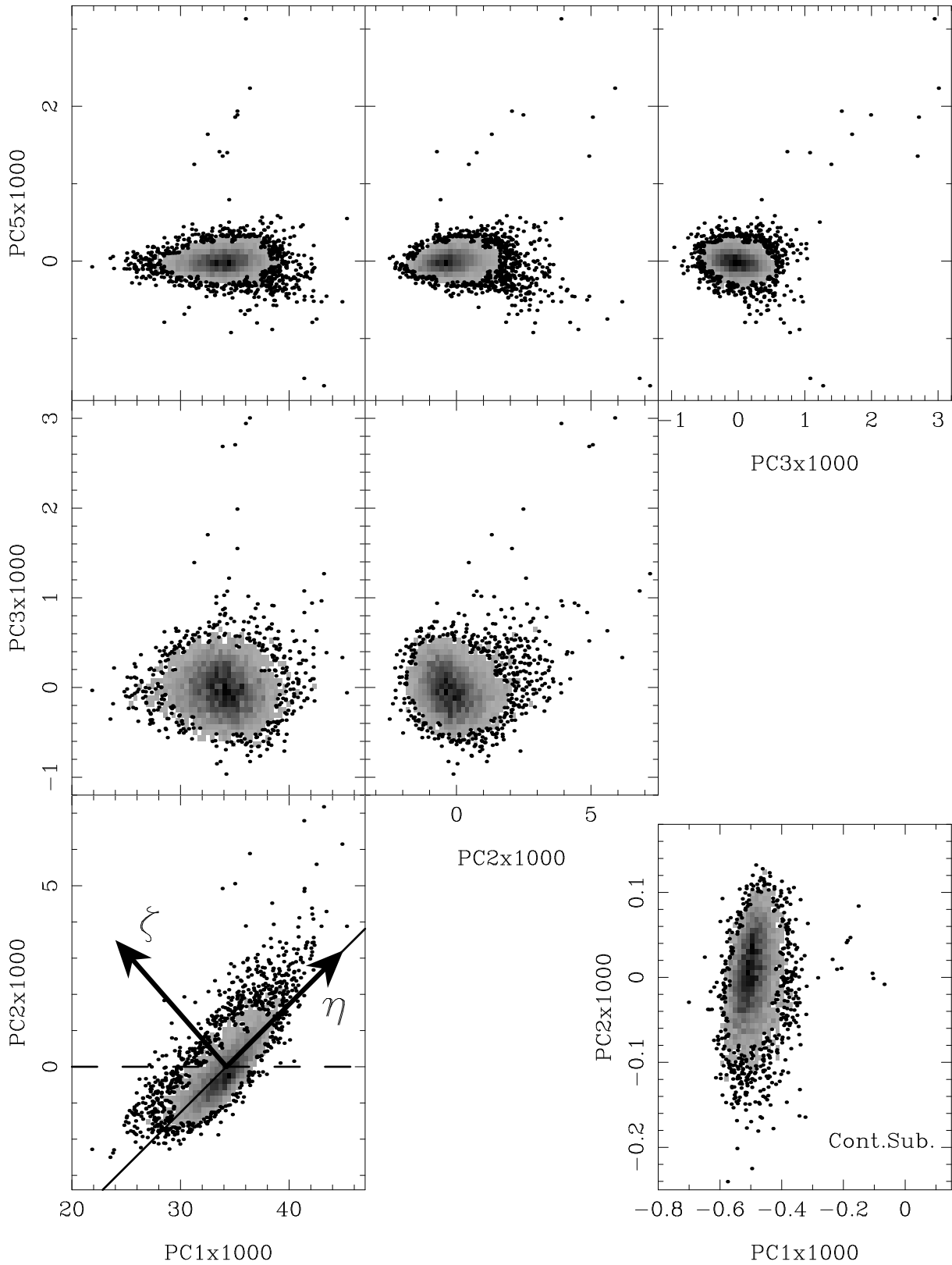
Figure 3. Projection of the galaxy spectra on principal components PC1, PC2, PC3 and PC5 ("flavour" 3 in table 1). The greyscale maps the number density of galaxies in PC-space. In the outer regions the greyscale is replaced by dots representing individual galaxies. The bottom-right panel gives the result for continuum subtracted spectra ("flavour" 4 in table 1). η and ζ are linear combinations of PC1 and PC2 which further separate the components.
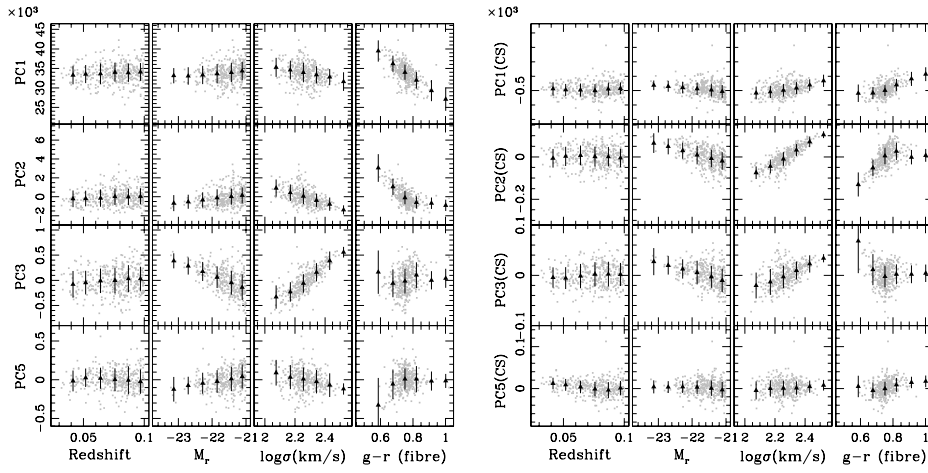
Figure 4. Correlation of the galaxy projections with respect to physical observables for the full spectra (*left*) and the continuum-subtracted SEDs (*right*). The black triangles and error bars give the average and standard deviation of the sample.
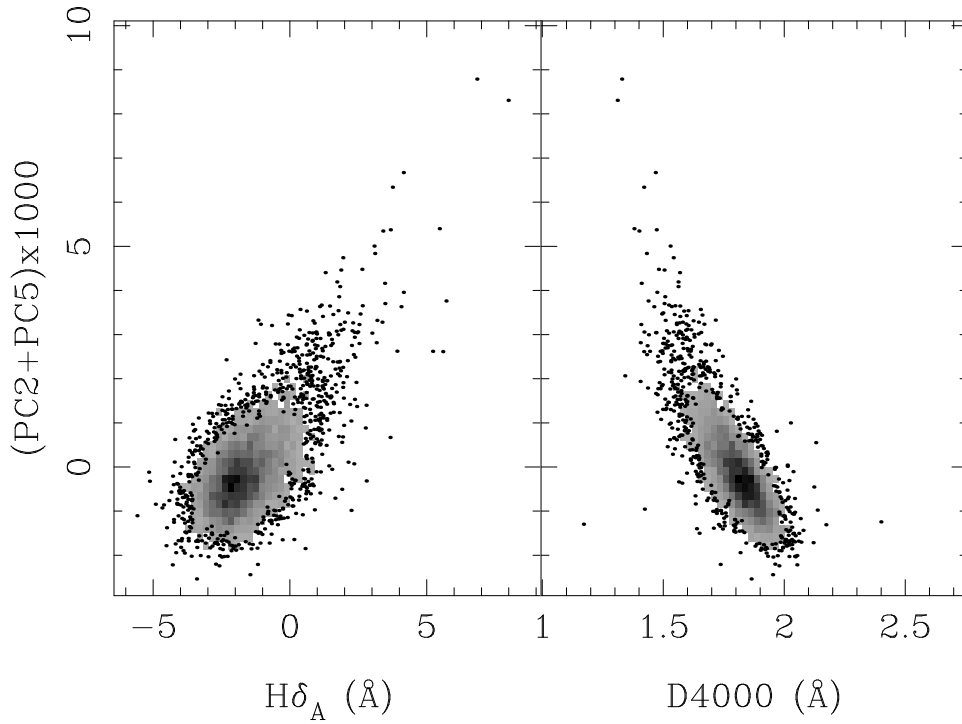
Figure 5. Correlation between a combination of PC2 and PC5 and the equivalent width of Hδ_A (*left*, as defined in Worthey & Ottaviani 1997); and the strength of the 4000Å break (*right*, as defined in Balogh et al. 1999).
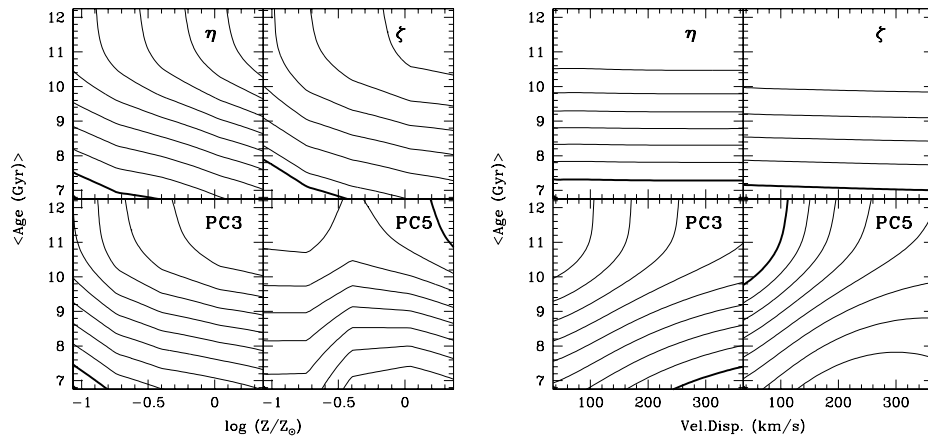
Figure 6. Synthetic spectra corresponding to an exponentially decaying star formation history at fixed metallicity are built using the Bruzual & Charlot (2003) models and projected on the principal components obtained for our sample. The figure shows contours of these projections with respect to average age and either metallicity (*left*) or velocity dispersion (*right*). The contour corresponding to the highest value is shown as a thick line. Notice η and ζ (or similarly PC1 and PC2) are insensitive to velocity dispersion, whereas PC3 is found to be strongly correlated with velocity dispersion (see table 2).
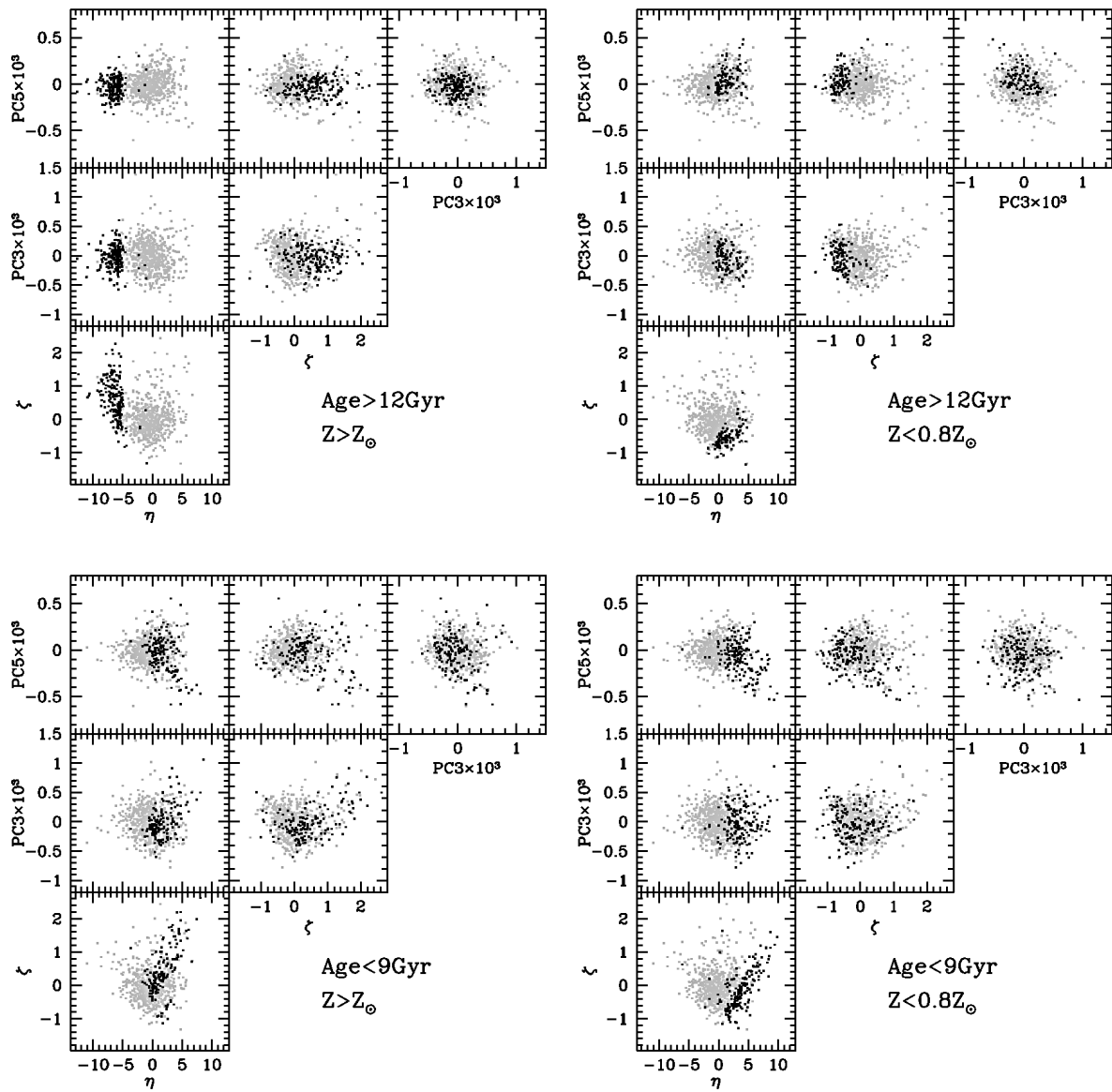
Figure 7. Comparison of the principal component projections with age/metallicity estimates using a direct fit to the full spectra via a χ^2 comparison with composite stellar populations from Bruzual & Charlot (2003) using an exponentially decaying star formation rate (see text for details). The grey dots show the total sample. The black dots correspond to subsamples which are best fit by models whose range of ages and metallicites are given in each panel.
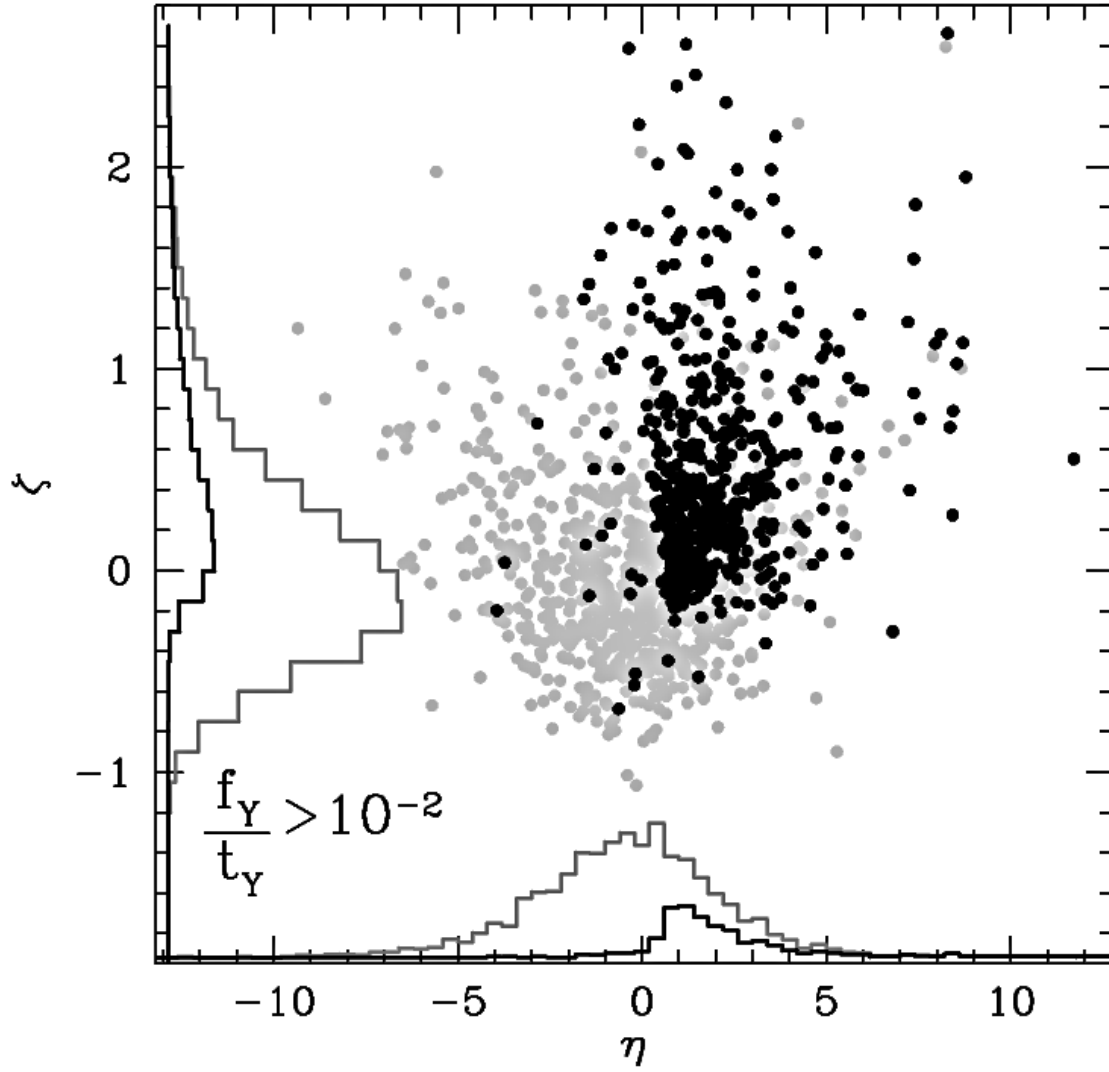
Figure 8. Comparison of the principal component projections with a model that overlays a young stellar population (age t_Y; mass fraction f_Y) on top of an old component (see text for details). The whole sample is shown as grey dots. The black dots correspond to galaxies whose best fit requires $f_Y/t_Y > 10^{-2}$ (e.g. 1% in 1 Gyr old stars). The histogram in the η and ζ parameters are shown for both sets of galaxies with the same colour coding.
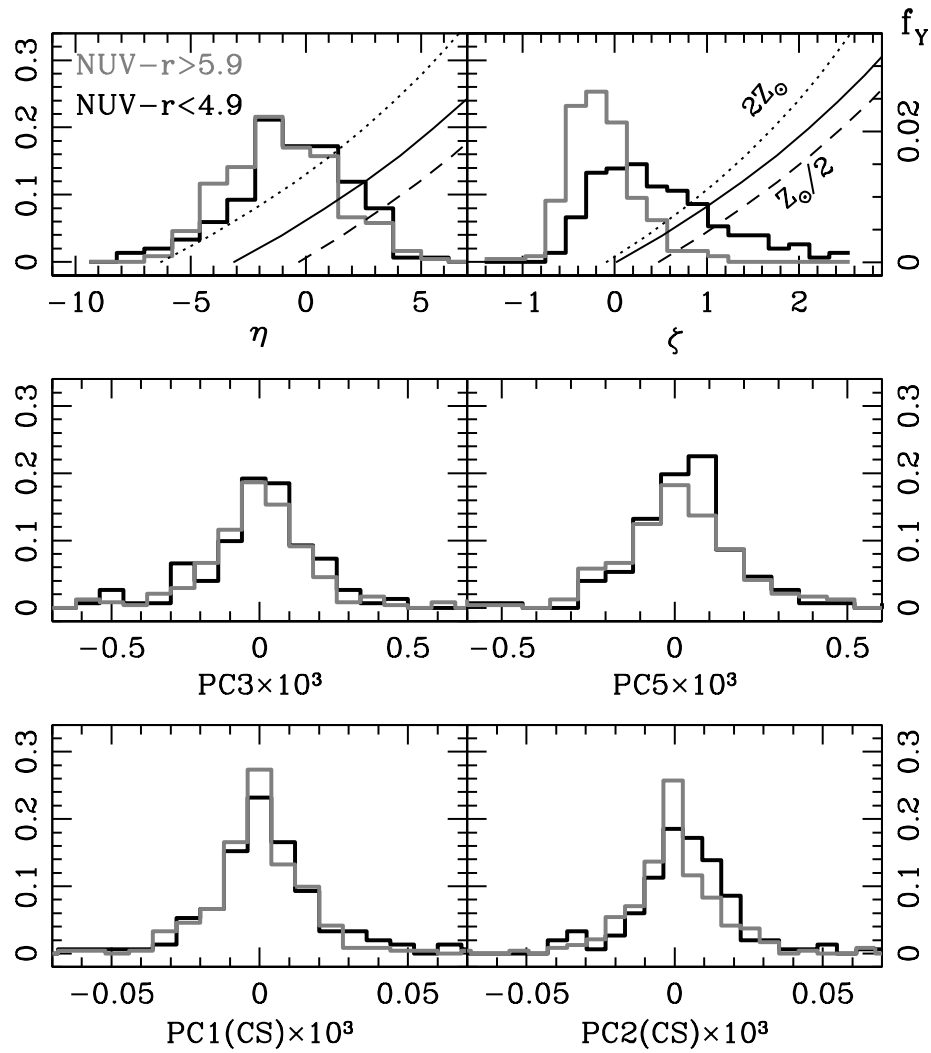
Figure 9. Distribution of the projections of the galaxy spectra on to our principal components. A subsample with available GALEX NUV data is chosen, and split according to NUV$-r$ colour. The NUV bright galaxies (black histograms) are expected to have undergone an episode of recent star formation (Schawinski et al. 2006). These galaxies have a different distribution of ζ but the distribution of the other components is indistinguishable from the red subsample. The bottom panels show the distribution of the projections of the first and second principal components for the continuum-subtracted case. Although small, there is a difference in the histogram of PC2 (which mainly relates to ζ for PCA with the full SEDs).
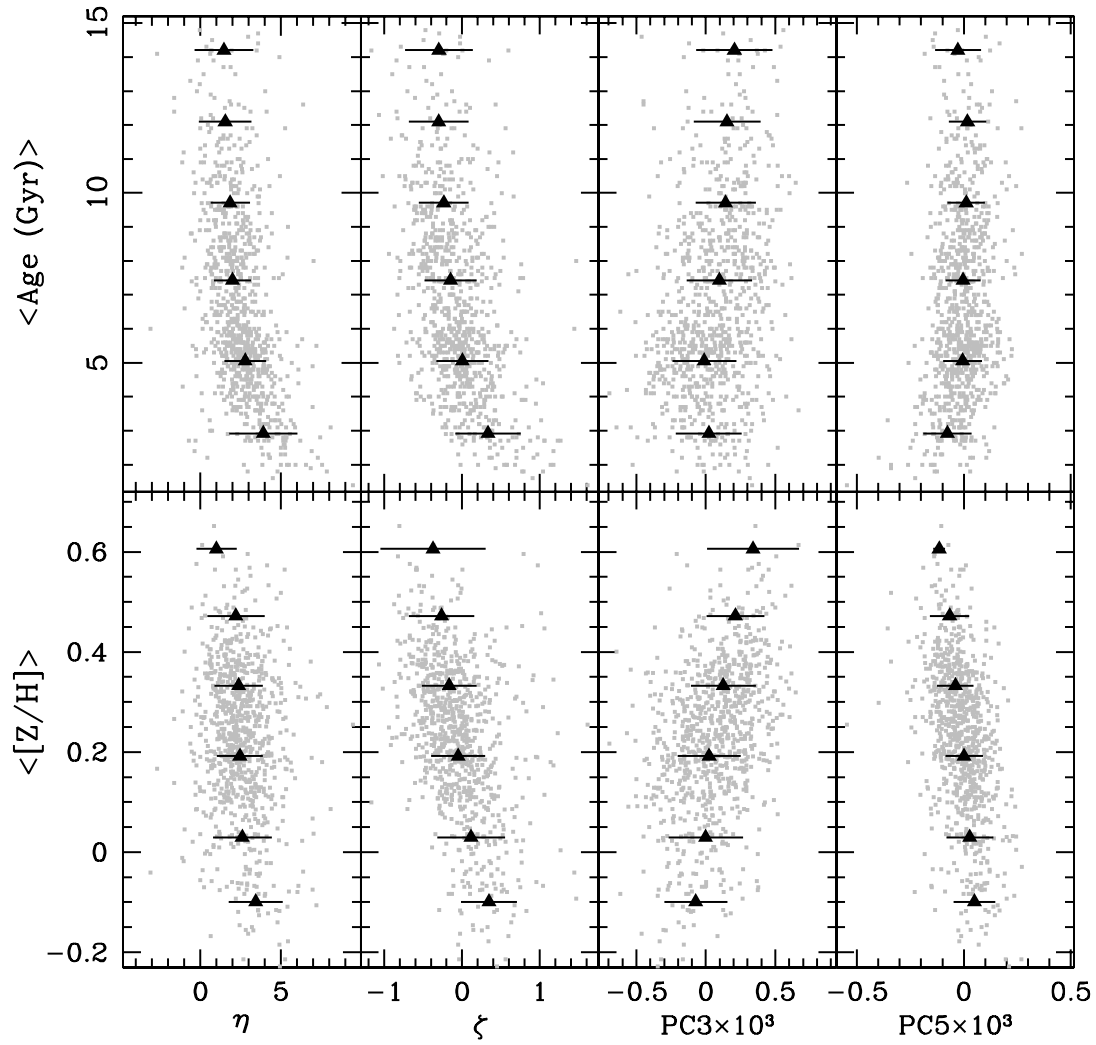
Figure 10. The composite spectra of Bernardi et al. (2006) are projected on our principal components. The age and metallicity estimates are presented in Bernardi et al. (2006) and are computed using a complete analysis of Lick indices and the Hγ absorption line. The triangles and error bars are average and standard deviation of data binned either in age or metallicity.
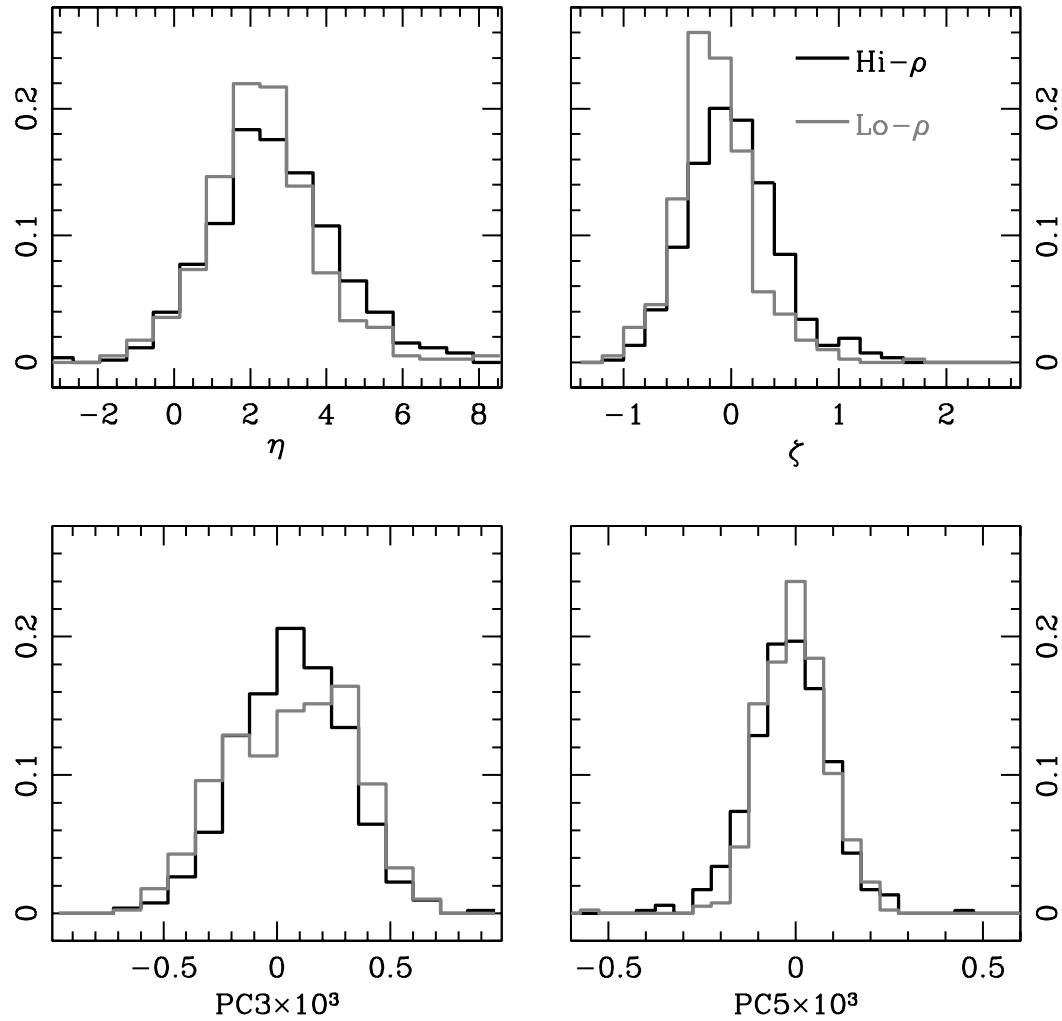
Figure 11. Comparison of the projections of the composite spectra on the principal components with respect to environment – as defined in Bernardi el al. (2006). Analogous to the results comparing distirbutions binned with respect to NUV$-r$ colours, the difference between galaxies in low and high density regions is found in the ζ parameter, with a skew towards high values for galaxies living in high-density regions.
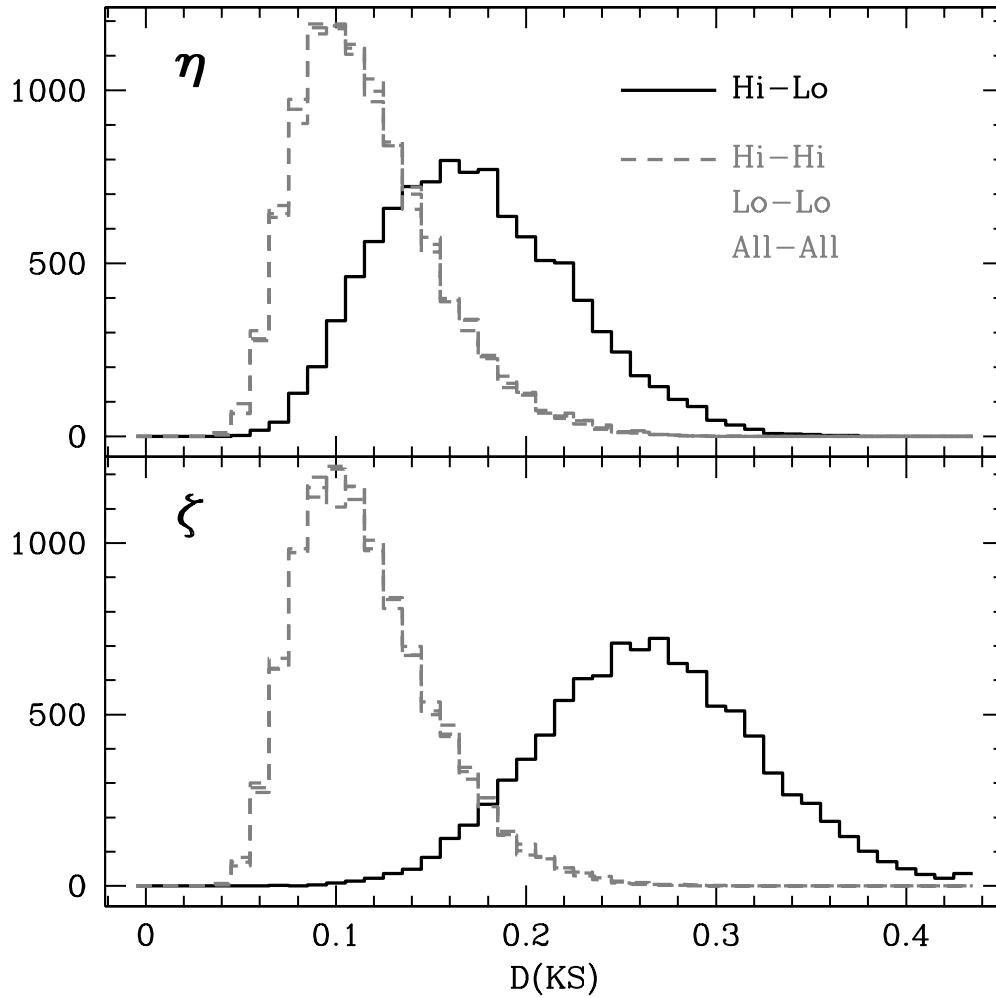
Figure 12. Checking the difference found between elliptical galaxies in high and low-density regions. The solid histograms show the distribution of the D-statistic from a Kolmogorov-Smirnov test applied to 10000 realisations on subsamples of 100 spectra each, extracted from the high and low-density samples. The dashed line histograms are similar distributions when extracted from the same density samples, either high; low-density or from the complete sample of composites.